Avrupa Bilim ve Teknoloji Dergisi
Özel Sayı 22, S. 282-292, Ocak 2021

Araştırma Makalesi

www.ejosat.com ISSN:2148-2683

European Journal of Science and Technology
Special Issue 22, pp. 282-292, January 2021

Research Article

Guidance and Control of a Surface-to-Surface Projectile Using a Nose Actuation Kit

Bülent Özkan[1], Harun Gökçe[2*]

[1] TÜBİTAK Defense Industries Research and Development Institute, Ankara, Turkey (ORCID: 0000-0003-3112-9723)
[2] TÜBİTAK Defense Industries Research and Development Institute, Ankara, Turkey (ORCID: 0000-0002-2702-0111)

(First received December 2020 and in final form January 2021)

(**DOI:** 10.31590/ejosat.848994)

ATIF/REFERENCE: Özkan, B. & Gökçe, H. (2021). Guidance and Control of a Surface-to-Surface Projectile Using a Nose Actuation Kit. *European Journal of Science and Technology*, (22), 282-292.

Abstract

Surface-to-surface projectiles are fired from ground launchers to specified ground targets to destroy them in an effective and economical manner. The mentioned munition is usually unguided and thus follows a ballistic trajectory. However, it is inevitable to have large miss distances when the diverting effects of the wind and thrust uncertainty are apparent. In this study, a gradual guidance and control strategy is proposed to improve the performance of this kind of munition. The effectiveness of this approach is shown by means of relevant computer simulations. The use of a simpler and cheaper nose actuation kit with pneumatic actuation makes this approach a preferable option for the application.

Keywords: Surface-to-surface projectile, guided projectile, guidance and control, nose actuation kit, thrust uncertainty.

Karadan Karaya Bir Merminin Burun Eyletim Kiti Kullanılarak Güdüm ve Denetimi

Öz

Karadan karaya mermiler, belirlenen yer hedeflerini etkin ve ekonomik bir şekilde tahrip etmek amacıyla, yerde konuşlu fırlatma platformlarından atılmaktadır. Bahsedilen mühimmat genellikle güdümsüz olup balistik bir yörüngeyi takip etmektedir. Öte yandan, rüzgâr ve itki belirsizliğinin neden olduğu olumsuz etkiler, mermilerin hedeften sapma miktarlarının artmasını kaçınılmaz kılmaktadır. Bu çalışmada, belirtilen tipteki mühimmatın başarım özelliklerini iyileştirmek amacıyla, kademeli bir güdüm ve denetim yaklaşımı önerilmektedir. Bahsedilen yöntemin etkinliği, gerçekleştirilen bilgisayar benzetimleri vasıtasıyla gösterilmeye çalışılmıştır. Oluşturulan şemanın pnömatik eyletimli basit yapıda ve ucuz bir burun kiti kullanılarak gerçekleniyor olması, sunulan yaklaşımı uygulamada tercih edilir bir seçenek olarak ortaya koymaktadır.

Anahtar Kelimeler: Satıhtan satha mühimmatlar, güdümlü mermi, güdüm ve kontrol, burun eyletim kiti, itme kararsızlığı.

[*] Corresponding Author: TÜBİTAK Defense Industries Research and Development Institute, Ankara, Turkey, ORCID: 0000-0002-2702-0111, *harungokce@yahoo.ca*

1. Introduction

Surface-to-surface projectiles (SSP's) have been widely used in military operations for long years. Ease of application and low cost advantages have made them a viable solution in land battles. They are usually provided with a high-rate continuous rotation around their longitudinal axis which is called "spin" from the beginning to the end of the trajectory to maintain their stability during the flight [1, 2]. On the other hand, since they are inherently unguided, the expected success levels occur below the expectations. Especially certain diverting effects including uncontrolled atmospheric phenomena such as wind and uncertainties on parameters and thrust make their performance decrease [1, 3, 4].

As per the current defence concepts, it is intended to hit the predefined target points without or at least with minimum collateral damage. In recent decades, this intention has led to the development and improvement of guided munition. While the munition with thrust is classified as rockets or missiles, the free-falling munition such as guided bombs are called as smart munition. Besides some of the guided munition is developed starting from the conceptual design phase as original systems, it is another common approach to convert general purpose munition into guided systems. The latter approach is usually applied on general purpose bombs. Apart from this, there is no obstacle on adapting this method to unguided SSP's to improve their performance characteristics. Despite their small mass resulting low amount of momentum effect during impact and relatively short range, low cost advantage of these projectiles makes this adaptation a viable option [1, 3, 4].

When unguided munition is equipped with guidance capability, it is observed that their performance is dramatically increased. Namely, the yielded miss distance to the target becomes very smaller than their unguided counterparts. Looking at the relevant studies, certain guidance approaches are suggested for light munition [5, 6].

In the literature, the following control approaches are encountered for controlling the unguided SSP's [1, 3, 4, 7]:

- Reaction jets,
- High-frequency piezo-electric actuators,
- Certain internal components of the munition,
- Nose actuation kit (NAK),
- Reverse rotation.

Using the approaches listed above, the trajectory of the projectile is tried to be diverted from its course to recover its nominal form which is distorted by certain external effects such as lateral wind. In fact, these methods are not often assisted by a certain guidance law. In few numbers of applications, an inertial guidance approach in which the SSP is directed towards the predefined path to the target as per the measurements of the critical kinematic parameters of the projectile including linear acceleration and angular speed components by means of certain onboard sensors is encountered. Here, what is primarily important to attain the desired control effectiveness is to adjust the control effort in a way that it does not cause an undesired instability due to high spin rates [8-11]. In this sense, none of those approaches except the NAK implementation utilizes a closed loop control scheme. That is, the relevant corrections are performed in an open loop manner on the desired trajectory. On the other hand, the usual SSP configuration involving a closed loop control system has only two control fins and thus its spatial effectiveness becomes quite limited.

In this study, a pneumatically-actuated add-on NAK consisting of two coupled fin pairs is proposed to make the control of the SSP's in accordance with a convenient guidance approach. Here, unlike the present control strategies over the guided SSP's as grouped above, a guidance strategy is considered as if the SSP were aimed at hitting a moving target. Namely, by means of a kinematic inversion point of view, the deviations on the trajectory of the missile due to external wind and/or thrust uncertainty are fictitiously transferred onto the target as if it behaved like a moving target law although it is stationary. For this purpose, the linear homing guidance (LHG) law is utilized for the mentioned motion planning of the projectile in its diving phase. Here, the main contribution of the present study is the application of a known guidance law along with a widely-used control scheme within an unusual strategy based on the kinematic inversion mentioned above upon the motion planning on the SSP's. In other words, despite the fact that this work does not have any claim on suggesting neither a new guidance method nor a control approach, it is aimed at showing the applicability and success of a guidance strategy which is originally utilized against moving targets on their stationary counterparts. At the end of the relevant computer simulations in which the unguided and guided projectile models are compared, it is testified that the guided projectile involving the proposed pneumatic NAK system results in comparatively small miss distances under even lateral wind effects.

2. Dynamic Modelling of the Projectile

The schematic representation of the considered unguided and guided projectiles are given in Figure 1 and Figure 2, respectively. As δ_a and δ_f stand for the fixed cant angle of the projectile and variable angular displacement of the control fins on NAK, respectively, NAK comprising four moveable control fins placed in "+" configuration is mounted in front of the unguided projectile body given in Figure 1 and Figure 2. Here, the horizontal fins are mutually coupled to constitute the elevator while the vertical ones are coupled to get the rudder. For the ease of control and cost effectiveness, the elevator and rudder are actuated pneumatically in bang-bang formation. Namely, the control fins rotate to limit values of the deflections angles, i.e. δ_f, only as per the angular commands sent by the controllers. In the mechanical sense, it is assumed that NAK can be screwed to the nose of the projectile. Thus, it becomes possible to remove the kit easily by unscrewing and changing it with a solid nose if desired.

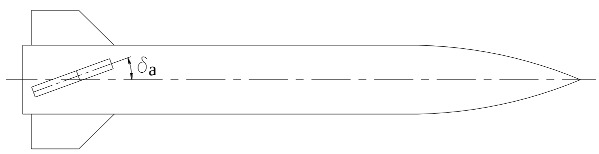

Figure 1. Unguided projectile geometry.

In the suggested use, the projectile is fired from a ground launcher with thrust and high-rate initial spin, and it remains climbing to its top point without control. Once it goes beyond the top point and begins diving, NAK switches on. The kit first attempts to nullify the high-rate spin by keeping the control fins at a fixed orientation which provides the projectile with roll motion in the sense opposite to the sense of the spin and then starts moving them in accordance with the commands generated by the guidance law.

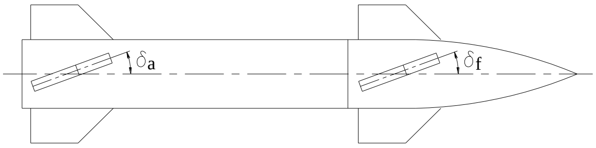

Figure 2. Guided projectile geometry.

As shown in Figure 3, the projectile is subjected to aerodynamic, Magnus, inertial, and thrust forces. Also, the aerodynamic moment resulted from the offset between the center of pressure upon which the aerodynamic and Magnus effect forces act (C_P) and mass center of the projectile (C_M) forces the projectile to move. The aerodynamic effects can be dealt with separately for steady and unsteady states. The thrust force is exerted on the projectile at the beginning of its motion and it burns out after a while very short compared to the total flight time [9-12].

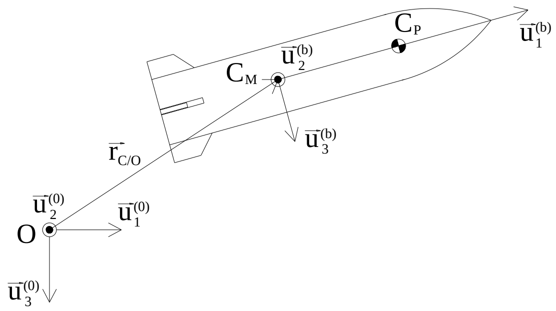

Figure 3. Guided projectile kinematics.

In Figure 3, as $j = 1,2 \; and \; 3$ and $\mathrm{k} = 0$ and b $\vec{u}_j^{(k)}$ denotes the unit vector indicating the j^{th} axis of F_0 and F_b which correspond to the earth-fixed reference frame with the origin of point O and projectile-fixed reference frame with the origin of point C_M, respectively. Furthermore, $\vec{r}_{c/0}$ stands for the relative position vector of point C_M with respect to point O.

The overall orientation of the projectile with respect to F_0 can be expressed using the rotated-frame-based yaw, pitch, and roll rotation sequence, i.e. 3-2-1 sequence, in the following manner [9-12]:

$$F_0 \xrightarrow[\psi]{\vec{u}_3^{(0)}} F_m \xrightarrow[\theta]{\vec{u}_2^{(m)}} F_n \xrightarrow[\varphi]{\vec{u}_1^{(n)}} F_b \tag{1}$$

In the sequence above ψ, θ, and ϕ represent the angular displacement variables of the projectile around the yaw, pitch, and roll axes, respectively. Moreover, F_M and F_n correspond to the intermediate frames between $F_0 - F_b$ transformation. Regarding the rotation sequence in equation (1), the overall transformation matrix from F_0 to F_b is obtained as a result of the forthcoming multiplication [13]:

$$\hat{C}^{(0,b)} = \hat{R}_3(\psi) \cdot \hat{R}_2(\theta) \cdot \hat{R}_1(\varphi) \tag{2}$$

The first, second, and third basic rotation matrices, i.e. $\hat{R}_1(\varphi)$, $\hat{R}_2(\theta)$, and $\hat{R}_3(\psi)$, in equation (2) are defined as follows [13]:

$$\hat{R}_1(\varphi) = \begin{bmatrix} 1 & 0 & 0 \\ 0 & cos(\varphi) & -sin(\varphi) \\ 0 & sin(\varphi) & cos(\varphi) \end{bmatrix} \tag{3}$$

$$\hat{R}_2(\theta) = \begin{bmatrix} cos(\theta) & 0 & sin(\theta) \\ 0 & 1 & 0 \\ -sin(\theta) & 0 & cos(\theta) \end{bmatrix} \tag{4}$$

$$\hat{R}_2(\Psi) = \begin{bmatrix} cos(\Psi) & -sin(\Psi) & 0 \\ -sin(\Psi) & cos(\Psi) & 0 \\ 0 & 0 & 1 \end{bmatrix} \tag{5}$$

As per the rotation sequence in equation (1), the angular velocity vector of the projectile with respect to F_0, i.e. $\vec{\omega}_{b/0}$, is determined using the following equality:

$$\vec{\omega}_{b/0} = \dot{\psi}\vec{u}_3^{(0)} + \dot{\theta}\vec{u}_2^{(m)} + \dot{\varphi}\vec{u}_1^{(n)} \tag{6}$$

Using the basic rotation matrices in equations (3) through (5), equation (6) can be expressed in terms of its components in F_0 as follows:

$$\begin{aligned} \bar{\omega}_{b/0}^{(0)} = {} & \left[-\dot{\theta}\, sin(\psi) + \dot{\varphi}\, cos(\psi)\, cos(\theta)\right]\bar{u}_1 \\ & + \left[\dot{\theta}\, cos(\psi) \right. \\ & \left. + \dot{\varphi}\, sin(\psi)\, cos(\theta)\right]\bar{u}_2 \\ & + \left[\dot{\psi} - \dot{\varphi}\, sin(\theta)\right]\bar{u}_3 \end{aligned} \tag{7}$$

where, as letter T indicates the matrix transpose, the column matrices of the unit vectrors are introduced as $\bar{u}_1 = [1 \quad 0 \quad 0]^T$, $\bar{u}_2 = [0 \quad 1 \quad 0]^T$, and $\bar{u}_3 = [0 \quad 0 \quad 1]^T$. $\vec{\omega}_{b/0}$ vector can be written in F_b as given below:

$$\bar{\omega}_{b/0}^{(b)} = [p \quad q \quad r]^T \tag{8}$$

where p, q, and r denote the angular velocity components of the projectile in the roll, pitch, and yaw directions, respectively. Taking the time derivative of equation (8) yields the column matrix representation of the angular acceleration vector of the projectile, i.e. $\vec{\alpha}_{b/0}$, in F_b.

$$\bar{\alpha}_{b/0}^{(b)} = [\dot{p} \quad \dot{q} \quad \dot{r}]^T \tag{9}$$

The column representation of the linear acceleration vector of point C_M, i.e. $\vec{a}_{C/O}$, in F_b is found by taking the time derivative of $\vec{r}_{C/O}$ twice:

$$\begin{aligned} \bar{a}_{C/O}^{(b)} = {} & (\dot{u} + qw - rv)\bar{u}_1 + (\dot{v} - pw + ru)\bar{u}_2 \\ & + (\dot{w} + pv - qu)\bar{u}_3 \end{aligned} \tag{10}$$

where u, v, and w denote the components of the linear velocity vector of C_M relative to O, i.e. $\vec{v}_{C/O}$, in F_b. Force and moment equations of the projectile are derived using the well-known Newton-Euler equalities:

$$\vec{F}_A + \vec{F}_M + \vec{W} + \vec{T} = m\vec{a}_{C/O} \tag{11}$$

$$\vec{M}_A + \vec{M}_U + \vec{M}_M + \vec{M} = \check{J}_C \cdot \vec{\alpha}_{b/0} + \vec{\omega}_{b/0} \times \check{J}_C \cdot \vec{\omega}_{b/0} \tag{12}$$

The following quantities are introduced in equations (11) and (12):

m : Mass of the projectile

$\check{J}_C$: Moment of inertia dyadic of the projectile about C_M

$\vec{F}_A$: Aerodynamic force vector

$\vec{F}_M$: Magnus force vector

$\vec{W}$: Weight vector of the projectile

$\vec{T}$: Thrust vector

$\vec{M}_A$: Steady aerodynamic moment vector

$\vec{M}_U$: Unsteady aerodynamic moment vector

$\vec{M}_M$: Magnus moment vector

$\vec{M}$: Thrust misalignment moment vector

$\vec{M}_A$ and $\vec{M}_M$ in equation (12) are the effects of $\vec{F}_A$ and $\vec{F}_M$ which act on the projectile at C_P on C_M, respectively. As the position vector of C_P relative to C_M is shown by $\vec{r}_{Cp/Cm}$, the forthcoming relationships are held for $\vec{M}_A$ and $\vec{M}_M$:

$$\vec{M}_A = \vec{r}_{Cp/Cm} \times \vec{F}_A \tag{13}$$

$$\vec{M}_M = \vec{r}_{Cp/Cm} \times \vec{F}_M \tag{14}$$

Equations (11) and (12) are expressed in the column matrix forms in F_b as follows:

$$\bar{F}_A^{(b)} + \bar{F}_M^{(b)} + \bar{W}^{(b)} + \bar{T}^{(b)} = m\bar{a}_{C/O}^{(b)} \tag{15}$$

$$\bar{M}_A^{(b)} + \bar{M}_U^{(b)} + \bar{M}_M^{(b)} + \bar{M}^{(b)} = \hat{J}_C^{(b)}\bar{\alpha}_{b/0}^{(b)} + \tilde{\omega}_{b/0}^{(b)}\hat{J}_C^{(b)}\bar{\omega}_{b/0}^{(b)} \tag{16}$$

As to be used to expand equations (15) and (16), the effective cross-sectional area of the projectile, dynamic pressure, angle of attack, and side-slip angle, i.e. S_P, q_∞, α, and β, can be formulated as functions of the diameter of the projectile, air density, and magnitude of the linear velocity vector of the projectile, i.e. d_p, ρ, and $v_p = \sqrt{u^2 + v^2 + w^2} = |\vec{v}_{C/O}|$) in the following manner by assuming $\pi = 3.14$:

$$S_P = (\pi/4)d_P^2 \tag{17}$$

$$q_\infty = (1/2)\rho v_P^2 \tag{18}$$

$$\alpha = a\,tan(w/v_P) \tag{19}$$

$$\beta = a\,tan(v/v_P) \tag{20}$$

As g represents the gravity ($g = 9.81\ m/s2$) and I_a and I_t correspond to the axial and lateral moment of inertia components of the projectile, the terms in equations (15) and (16) can be expanded as follows [4, 11, 14]:

$$\hat{J}_C^{(b)} = \begin{bmatrix} I_a & 0 & 0 \\ 0 & I_t & 0 \\ 0 & 0 & I_t \end{bmatrix} \tag{21}$$

$$\tilde{\omega}_{b/0}^{(b)} = \begin{bmatrix} 0 & -r & q \\ r & 0 & -p \\ -q & p & 0 \end{bmatrix} \tag{22}$$

$$\bar{F}_A^{(b)} = q_\infty S_P \begin{bmatrix} C_{x0} \\ C_{y\beta}\beta + C_{y_\delta}\delta_r + C_{yr}[d_P/(2v_P)]r \\ C_{z\alpha}\alpha + C_{z_\delta}\delta_e + C_{zq}[d_P/(2v_P)]q \end{bmatrix} \tag{23}$$

$$\bar{F}_M^{(b)} = q_\infty S_P \begin{bmatrix} 0 \\ C_{MFy}[d_P/(2v_P)]\alpha p \\ C_{MFz}[d_P/(2v_P)]\beta p \end{bmatrix} \tag{24}$$

$$\bar{W}^{(b)} = mg \begin{bmatrix} -sin(\theta) \\ cos(\theta)\,sin(\varphi) \\ cos(\theta)\,cos(\varphi) \end{bmatrix} \tag{25}$$

$$\bar{T}^{(b)} = [X_T \quad Y_T \quad Z_T]^T \tag{26}$$

$$\bar{M}_A^{(b)} = q_\infty S_P d_P \begin{bmatrix} C_{l0} \\ C_{m\alpha}\alpha + C_{m_\delta}\delta_e + C_{mq}[d_P/(2v_P)]q \\ C_{n\beta}\beta + C_{n_\delta}\delta_r + C_{nr}[d_P/(2v_P)]r \end{bmatrix} \tag{27}$$

$$\bar{M}_U^{(b)} = q_\infty S_P d_P \begin{bmatrix} C_{lU0} + C_{lUp}[d_P/(2v_P)]p \\ C_{MUq}[d_P/(2v_P)]q \\ C_{MUr}[d_P/(2v_P)]r \end{bmatrix} \tag{28}$$

$$\bar{M}_M^{(b)} = q_\infty S_P d_P \begin{bmatrix} 0 \\ C_{MTm}[d_P/(2v_P)]\alpha p \\ C_{MTn}[d_P/(2v_P)]\beta p \end{bmatrix} \tag{29}$$

$$\bar{M}^{(b)} = [L_T \quad M_T \quad N_T]^T \tag{30}$$

where X_T, Y_T, and Z_T denote the components of the thrust vector while L_T, M_T, and N_T indicate the components of the thrust misalignment moment vector in the directions of $\vec{u}_1^{(b)}$, $\vec{u}_2^{(b)}$, and $\vec{u}_3^{(b)}$ unit vectors in F_b, respectively. Also, δ_r and δ_e correspond to the rudder and elevator angles of the projectile.

The following relationships can be established among the aerodynamic coefficients C_{x0}, $C_{y\beta}$, $C_{y\delta}$, C_{yr}, $C_{z\delta}$, $C_{z\alpha}$, C_{zq}, C_{MFy}, C_{MFz}, C_{l0}, $C_{m\alpha}$, $C_{m\delta}$, C_{mq}, $C_{n\beta}$, $C_{n\delta}$, C_{nr}, C_{lu0}, C_{lup}, C_{Muq}, C_{Mur}, C_{MTm}, and C_{MTn} in equations (23), (24), (27), (28), and (29) thanks to the rotational symmetry of the projectile [15]:

$$C_{y\beta} = C_{z\alpha} \tag{31}$$

$$C_{y\delta} = -C_{z\delta} \tag{32}$$

$$C_{yr} = -C_{zq} \tag{33}$$

$$C_{n\beta} = -C_{m\alpha} \tag{34}$$

$$C_{n\delta} = C_{m\delta} \tag{35}$$

$$C_{nr} = C_{mq} \tag{36}$$

$$C_{MFy} = C_{MFz} \tag{37}$$

$$C_{MUr} = C_{MUq} \tag{38}$$

$$C_{MTn} = C_{MTm} \tag{39}$$

Substituting equations (21) through (39) into equations (15) and (16) and then making the necessary arrangements, the equations of motion defining the spatial motion of the projectile come into the picture as given below

$$\dot{u} + qw - rv = d_x + (X_T/m) - g\,sin(\theta) \tag{40}$$

$$\dot{v} - pw + ru = d_{z\alpha}\beta + d_{z\delta}\delta_r - d_{zq}r + d_{zp}\alpha p + (Y_T/m) + g\,cos(\theta)\,sin(\varphi) \tag{41}$$

$$\dot{w} + pv - qu = d_{z\alpha}\alpha + d_{z\delta}\delta_e + d_{zq}q + d_{zp}\beta p + (Z_T/m) + g\,cos(\theta)\,cos(\varphi) \tag{42}$$

$$\dot{p} = d_l + d_{lp}p + (L_T/I_a) \tag{43}$$

$$\dot{q} + [(I_a/I_t) - 1]pr = d_{m\alpha}\alpha + d_{m\delta}\delta_e + d_{mq}q + d_{mp}\alpha p + (M_T/I_t) \tag{44}$$

$$\dot{r} - [(I_a/I_t) - 1]pq = -d_{m\alpha}\beta + d_{m\delta}\delta_r + d_{mq}r + d_{mp}\beta p + (N_T/I_t) \tag{45}$$

where $d_x = q_\infty S_P C_{x0}/m$, $d_{z\alpha} = q_\infty S_P C_{z\alpha}/m$, $d_{z\delta} = q_\infty S_P C_{z\delta}/m$, $d_{zq} = (q_\infty S_P d_P C_{zq})/(2mv_P)$, $d_{zp} = (q_\infty S_P d_P C_{MFz})/(2mv_P)$, $d_l = q_\infty S_P d_P (C_{l0} + C_{lU0})/I_a$, $d_{lp} = (q_\infty S_P d_P^2 C_{lUp})/(2I_a v_P)$, $d_{m\alpha} = q_\infty S_P d_P C_{m\alpha}/I_t$, $d_{m\delta} = q_\infty S_P d_p C_{m\delta}/I_t$,

$d_{mq} = [q_\infty S_P d_P^2 (C_{mq} + C_{MUq})]/(2I_t v_P),$
$d_{mp} = (q_\infty S_P d_P^2 C_{MTm})/(2I_t v_P).$

Here, as $C_{l\delta}$ stands for the relevant stability derivative, C_{l0} can approximately be defined as a linear function of δ_a:

$$C_{l0} = C_{l\delta}\delta_a \quad (46)$$

3. Guidance Law

As per a basis is establish for the guidance scheme, the engagement geometry between the projectile and target can be described by the following relationships where $r_{T/P}$ indicates the distance between the projectile and target while λ_p and λ_y denote the orientation angles of $r_{T/P}$ with respect to the pitch and yaw planes, respectively [16]:

$$r_{T/P} = \sqrt{\Delta x^2 + \Delta y^2 + \Delta z^2} \quad (47)$$

$$\lambda_p = arctan[-\Delta z\, cos(\lambda_y)/\Delta x] \quad (48)$$

$$\lambda_y = arctan(\Delta y/\Delta x) \quad (49)$$

The total miss distance at the end of the engagement, i.e. d_{miss}, at $t = t_F$ where t_F represents the final time of the engagement can be calculated from the following formula just as the vertical component of $r_{T/P}$ becomes zero, i.e. $\Delta z = 0$ [16].

$$d_{miss} = \sqrt{\Delta x^2(t_F) + \Delta y^2(t_F)} \quad (50)$$

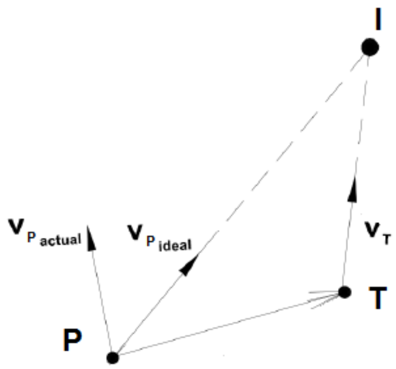

Figure 4. Linear homing guidance geometry.

The motion planning of the projectile is carried out in accordance with the LHG law for the terminal flight phase starting right after the roll nullification. In the LHG law whose schematic representation is submitted in Figure 4, as the projectile (*P*), target (*T*), and predicted intercept point (*I*) form a triangular shape called the collision tirangle whose dimensions are continuously updated during the engagement, the objective is first to put and then to keep the velocity vector of the object on the fictitious line connecting the object and predicted intercept point on the collision triangle. In Figure 4, the symbols $v_{Pactual}$ and v_{Pideal} denote the actual and desired velocity vectors of the projectile while v_T indicates the target velocity vector. In this approach, in order for point *P* to catch point *T*, the guidance commands can be derived in terms of the flight path angles of the projectile which are the orientation angles of $\vec{v}_{C/O}$ from the lateral and vertical axes of F_0, i.e. η_q^c and γ_q^c, in the following manner [16]:

$$\eta_q^c = a\,tan[(v_{Ty}\Delta t - \Delta y)/(v_{Tx}\Delta t - \Delta x)] \quad (51)$$

$$\gamma_q^c = a\,tan\{(\Delta z - v_{Tz}\Delta t) /[(v_{Tx}\Delta t - \Delta x)\,cos(\eta_q^c) + (v_{Ty}\Delta t - \Delta y)\,sin(\eta_q^c)]\} \quad (52)$$

As x_c, y_c, and z_c denote the components of $\vec{r}_{C/O}$in F_0 while x_T, y_T, and z_T are used to indicate the linear position vector components of the target point relative to point O in F_0, the definitions made in equations (51) and (52) are revealed below by introducing the velocity components of the target in F_0 as v_{Tx}, v_{Ty}, and v_{Tz} as well as the magnitude of the target velocity vector of v_T [16]:

$$\Delta x = x_C - x_T \quad (53)$$

$$\Delta y = y_C - y_T \quad (54)$$

$$\Delta z = z_C - z_T \quad (55)$$

$$v_{Tx} = v_T\,cos(\gamma_t) \quad (56)$$

$$v_{Ty} = v_T\,sin(\gamma_t) \quad (57)$$

$$v_{Tz} = 0 \quad (58)$$

Where γ_t denotes the flight path angle of the target on the horizontal plane of F_0. Furthermore, the remaining time duration till the end of the engagement, i.e. Δt, is found below [16]:

$$\Delta t = \left[\sqrt{\sigma^2 + (v_C^2 - v_T^2)\Delta r^2} - \sigma\right]/(v_C^2 - v_T^2) \quad (59)$$

where $\sigma = v_{Tx}\Delta x + v_{Ty}\Delta y + v_{Tz}\Delta z$ and $\Delta r^2 = \Delta x^2 + \Delta y^2 + \Delta z^2$. In the present problem, the projectile is fired towards a stationary ground target. Therefore, v_T is zero. This condition simplifies the general form of the LHG law explained above regarding the case.

4. Projectile Control System

The guidance commands generated by the LHG law in terms of the flight path angle components of the projectile can be converted into physical motion by means of a conveniently designed control system, i.e. autopilot. For this purpose, regarding that the high-rate spin of the projectile, i.e. roll rate, is almost nullified primarily at the beginning of the guidance and control phase ($p \approx 0$), equations (41), (42), (44), and (45) can be reduced to the following forms:

$$\dot{v} + ru = d_{z\alpha}\beta + d_{z\delta}\delta_r - d_{zq}r + (Y_T/m) + g\,cos(\theta)\,sin(\varphi) \quad (60)$$

$$\dot{w} - qu = d_{z\alpha}\alpha + d_{z\delta}\delta_e + d_{zq}q + (Z_T/m) + g\,cos(\theta)\,cos(\varphi) \quad (61)$$

$$\dot{q} = d_{m\alpha}\alpha + d_{m\delta}\delta_e + d_{mq}q + (M_T/I_t) \quad (62)$$

$$\dot{r} = -d_{m\alpha}\beta + d_{m\delta}\delta_r + d_{mq}r + (N_T/I_t) \quad (63)$$

Since the thrust effect burns out before the guided phase of the projectile, the relevant force and moment terms vanish in the equations of motion. Apart from this, evaluating the gravity effect as a constant bias, or disturbing effect, on the control system, equations (60) through (63) are more simplified as follows:

$$\dot{v} + ru = d_{z\alpha}\beta + d_{z\delta}\delta_r - d_{zq}r \quad (64)$$

$$\dot{w} - qu = d_{z\alpha}\alpha + d_{z\delta}\delta_e + d_{zq}q \quad (65)$$

$$\dot{q} = d_{m\alpha}\alpha + d_{m\delta}\delta_e + d_{mq}q \quad (66)$$

$$\dot{r} = -d_{m\alpha}\beta + d_{m\delta}\delta_r + d_{mq}r \quad (67)$$

The longitudinal component of $\vec{v}_{C/O}$ in F_b, i.e. u, is much larger than its lateral components, i.e. v and w. Thus, the following approximation upon u can be taken into consideration along with the small angle equivalents of α and β as introduced in equations (19) and (20) in the autopilot design:

$$u \approx |\vec{v}_{C/O}| = v_P \quad (68)$$

$$w \approx u\alpha \quad (69)$$

$$v \approx u\beta \quad (70)$$

Ignoring the change of u in time, first time derivatives equations (69) and (70) yield the next expressions:

$$\dot{w} \approx u\dot{\alpha} \quad (71)$$

$$\dot{v} \approx u\dot{\beta} \quad (72)$$

Plugging equations (69) through (72) into equations (64) through (67), the following scalar relationships are obtained:

$$\dot{\beta} = -c_{\alpha q}r + c_{\alpha\alpha}\beta - c_{\alpha\delta}\delta_r \quad (73)$$

$$\dot{\alpha} = c_{\alpha q}q + c_{\alpha\alpha}\alpha + c_{\alpha\delta}\delta_e \quad (74)$$

$$\dot{q} = d_{mq}q + d_{m\alpha}\alpha + d_{m\delta}\delta_e \quad (75)$$

$$\dot{r} = d_{mq}r - d_{m\alpha}\beta + d_{m\delta}\delta_r \quad (76)$$

where $c_{\alpha q} = (d_{zq}/v_P) + 1$, $c_{\alpha\alpha} = d_{z\alpha}/v_P$, and $c_{\alpha\delta} = d_{z\delta}/v_P$. Noting that $\dot{\theta} \approx q$ and $\dot{\psi} \approx r$, the differential equations governing the motion of the projectile in the pitch and yaw planes can be gathered in the forthcoming state space forms:

$$\dot{\bar{x}}_p = \hat{A}_p\bar{x}_p + \bar{b}_p\delta_e \quad (77)$$

$$\dot{\bar{x}}_y = \hat{A}_y\bar{x}_y + \bar{b}_y\delta_r \quad (78)$$

where, as the column representations of the state variable vectors for the pitch and yaw planes are introduced to be $\bar{x}_p = [\theta \quad q \quad \alpha]^T$ and $\bar{x}_y = [\psi \quad r \quad \beta]^T$, respectively,

$$\hat{A}_p = \begin{bmatrix} 0 & 1 & 0 \\ 0 & d_{mq} & d_{m\alpha} \\ 0 & c_{\alpha q} & c_{\alpha\alpha} \end{bmatrix}, \bar{b}_p = [0 \quad d_{m\delta} \quad c_{\alpha\delta}]^T,$$

$$\hat{A}_y = \begin{bmatrix} 0 & 1 & 0 \\ 0 & d_{mq} & -d_{m\alpha} \\ 0 & -c_{\alpha q} & c_{\alpha\alpha} \end{bmatrix}, \text{and } \bar{b}_y = [0 \quad d_{m\delta} \quad -c_{\alpha\delta}]^T.$$

The input variables δ_e and δ_r can be designated as per the state feedback approach as follows:

$$\delta_e = k_\theta(\theta_d - \theta) - k_q q - k_\alpha\alpha \quad (79)$$

$$\delta_r = k_\psi(\psi_d - \psi) - k_r r - k_\beta\beta \quad (80)$$

In equations (79) and (80), θ_d and ψ_d denote the desired values of θ and ψ, respectively. Also, k_θ, k_q, k_α, k_ψ, k_r, and k_β are assigned as the controller gains. Defining the reference inputs for the pitch and yaw planes as $r_p = \theta_d$ and $r_y = \psi_d$, equations (79) and (80) can be expressed more compactly as shown below:

$$\delta_e = -\bar{k}_p^T\bar{x}_p + k_\theta r_p \quad (81)$$

$$\delta_r = -\bar{k}_y^T\bar{x}_y + k_\psi r_y \quad (82)$$

where $\bar{k}_p = [k_\theta \quad k_q \quad k_\alpha]^T$ and $\bar{k}_y = [k_\psi \quad k_r \quad k_\beta]^T$. Eventually, inserting equations (81) and (82) into equations (77) and (78), the state space representations of the closed loop pitch and yaw autopilots come into the picture in the following fashion:

$$\dot{\bar{x}}_p = (\hat{A}_p - \bar{b}_p\bar{k}_p^T)\bar{x}_p + k_\theta\bar{b}_p r_p \quad (83)$$

$$\dot{\bar{x}}_y = (\hat{A}_y - \bar{b}_y\bar{k}_y^T)\bar{x}_y + k_\psi\bar{b}_y r_y \quad (84)$$

Having applied the laplace transformation to equations (83) and (84), the characteristics polynomials of the resulting transfer functions of the pitch and yaw planes are obtained. Then, equating these polynomials to the standard third order characteristic polynomial $B_3(s)$ given in equation (85) for $i = p$ and y, the controller gains appear as in equations (86) and (87):

$$B_3(s) = s^3 + (2\zeta_i + 1)\omega_{ic}s^2 + (2\zeta_i + 1)\omega_{ic}^2 s + \omega_{ic}^3 \quad (85)$$

$$\bar{k}_p = \hat{C}_p^{-1}\bar{d}_p \quad (86)$$

$$\bar{k}_y = \hat{C}_y^{-1}\bar{d}_y \quad (87)$$

where ω_{ic} and ζ_i stand for the desired bandwidth and damping ratio for the pitch and yaw planes. Also;

$$\hat{C}_p = \begin{bmatrix} 0 & d_{m\delta} & c_{\alpha\delta} \\ d_{m\delta} & c_{\alpha\delta}d_{m\alpha} - c_{\alpha\alpha}d_{m\delta} & c_{\alpha q}d_{m\delta} - c_{\alpha\delta}d_{mq} \\ c_{\alpha\delta}d_{m\alpha} - c_{\alpha\alpha}d_{m\delta} & 0 & 0 \end{bmatrix},$$

$$\bar{d}_p = \begin{bmatrix} (2\zeta_p + 1)\omega_{pc} + d_{mq} + c_{\alpha\alpha} \\ (2\zeta_p + 1)\omega_{pc}^2 + c_{\alpha q}d_{m\alpha} - c_{\alpha\alpha}d_{mq} \\ \omega_{pc}^3 \end{bmatrix},$$

$$\hat{C}_y = \begin{bmatrix} 0 & d_{m\delta} & -c_{\alpha\delta} \\ d_{m\delta} & c_{\alpha\delta}d_{m\alpha} - c_{\alpha\alpha}d_{m\delta} & c_{\alpha\delta}d_{mq} - c_{\alpha q}d_{m\delta} \\ c_{\alpha\delta}d_{m\alpha} - c_{\alpha\alpha}d_{m\delta} & 0 & 0 \end{bmatrix},$$

and $\bar{d}_y = \begin{bmatrix} (2\zeta_y + 1)\omega_{yc} + d_{mq} + c_{\alpha\alpha} \\ (2\zeta_y + 1)\omega_{yc}^2 + c_{\alpha q}d_{m\alpha} - c_{\alpha\alpha}d_{mq} \\ \omega_{yc}^3 \end{bmatrix}$.

The standard third-order characteristic polynomial puts the three poles of the closed loop pitch and yaw autopilots on the left-hand-side of the complex plane. Thus, the asymptotical stabilities of these autopilots, i.e. control systems, are guaranteed by updating the values of the aerodynamic coefficients in accordance with the instantaneous state of the flight.

Different from electro-mechanical or hydraulic actuation, the control fins rotate at amount of either $-\delta_f$ or δ_f. Regardless their magnitudes, the signs of δ_e and δ_r define the sign of δ_f. Thus, the command signals, i.e. δ_e' and δ_r', are sent to the pneumatic control fins by the pitch and yaw autopilots in the following forms:

$$\delta_e' = sign(\delta_e)\delta_f \quad (88)$$

$$\delta_r' = sign(\delta_r)\delta_f \quad (89)$$

5. Computer Simulations

In the computer simulations, the performance characteristics of three projectile configurations are examined:

- Unguided projectile with zero cant angle (U-Z),
- Unguided projectile with nonzero cant angle (U-N),
- Guided projectile with zero cant angle (G).

That is, the unguided, i.e., ballistic, projectiles are considered for both uncanted and canted fixed tail fins configurations while the guided projectile is taken to be in an uncanted manner. Here, the fixed cant angle, i.e., δ_a, is assigned to be 0.5°. Also, the magnitude of the net orientation angle defined as the difference between δ_a and δ_e/δ_r is set to be -5° for the high-rate spin nullification phase whereas the upper and lower limits of the pneumatically actuated control fins, i.e., δ_f are adjusted to be ±1° for the guidance phase. The engagement scenarios are designed regarding the uncontrolled lateral wind effect in addition to the thrust uncertainty. In this designation, it is assumed that the wind affects the projectile at altitudes which are higher than the half of the top point the projectile can attain. The relevant aerodynamic coefficients including the Magnus force and moment terms are obtained using the look-up tables prepared special for the considered situations. Also, all the simulations are terminated once the relative altitude between the projectile and target point drops down 0.5 m.

The numerical values of the projectile parameters used in the simulations are shown in Table 1.

Table 1. Essential parameters for the projectile.

Parameter	Symbol	Value
Diameter	d_P	70 mm
Cross-Sectional Area	S_P	3,848.5 mm^2
Total Length	L_P	2,000 mm
Total Mass	m	15 kg
Axial Moment of Inertia	I_a	0.018 kg·m^2
Transversal Moment of Inertia	I_t	5.005 kg·m^2

Under the stated conditions, the attained results for the engagement time and miss distance quantities are submitted in Table 2 and Table 3 for the initial pitch angle, i.e. θ, values of 30 and 45°. In these scenarios, lateral wind speed is assumed to be 0, 10, and 30 m/s [7]. Apart from these issues, −10% of thrust uncertainty is taken into account as in the related simulation data in Table 3.

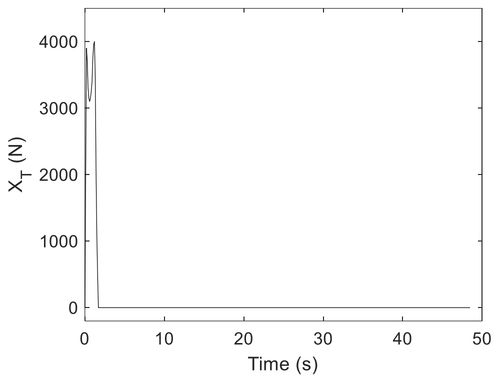

Figure 5. Thrust profile.

The reference ranges of the guided projectile configuration are determined as per the estimated range of the unguided projectile with zero cant angle. As seen from the profile given in Figure 5, the thrust burns out at 1.7 s after the launch for all the cases considered. Also, the engagement geometries are submitted in Figure 6 through Figure 15 as well as sample time response graphs. In all the cases, the initial speed of the projectile is taken to be 408 m/s.

Table 2. Results for θ=30 and 45° without thrust uncertainty.

Case Number	Lateral Wind Speed (m/s)	Projectile Configuration	Estimated Distance to Target (m)	Engagement Time (s)	Miss Distance (m)		
					Lateral	Longitudinal	Resultant
θ=30°							
1	0	U-Z	10,735	34	0	37	37
2		U-N	10,783	34	0	4	4
3		G	10,735	34	0	-39	39
θ=45°							
4	0	U-Z	12,291	48	0	-51	51
5		U-N	12,259	48	0	-6	6
6		G	12,291	48	0	-69	69
7	10	U-Z	12,291	48	-1	48	48
8		U-N	12,259	50	1,352	277	1,380
9		G	12,291	48	0	-74	74
10	30	U-Z	12,291	49	13	1,052	1,052
11		U-N	12,259	54	2,644	581	2,707
12		G	12,291	46	0	-69	69

Table 3. Results for θ=45° with thrust uncertainty of −10%.

Case Number	Lateral Wind Speed (m/s)	Projectile Configuration	Estimated Distance to Target (m)	Engagement Time (s)	Miss Distance (m)		
					Lateral	Longitudinal	Resultant
13	0	U-Z	12,291	43	0	-2,838	2,838
14		U-N	12,259	43	-21	2,784	2,784
15		G	12,291	53	0	-98	98
16	10	U-Z	12,291	43	0	-2,785	2,785
17		U-N	12,259	43	-394	-2,922	2,948
18		G	12,291	53	0	-86	86
19	30	U-Z	12,291	43	-14	-2,382	2,382
20		U-N	12,259	44	-571	-2,236	2,308
21		G	12,291	51	0	-135	135

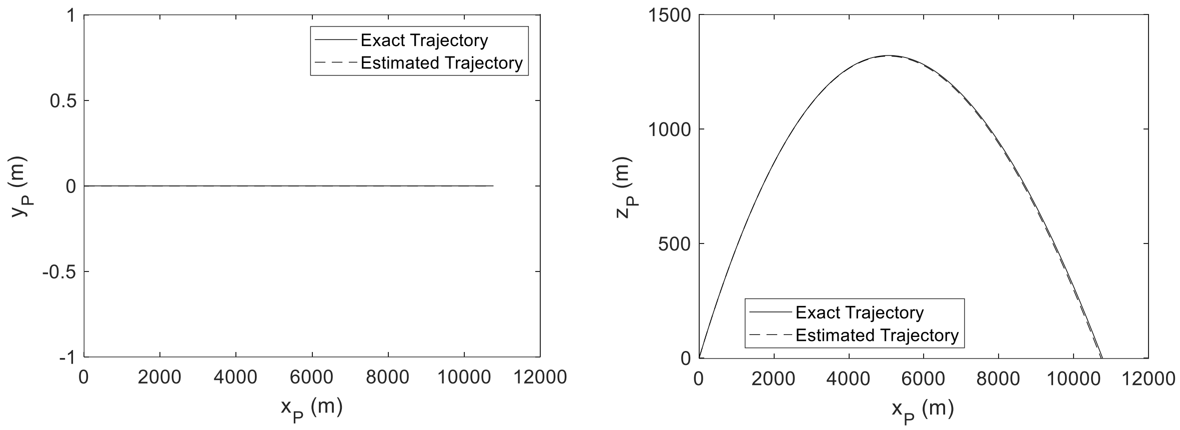

Horizontal Engagement *Vertical Engagement*

Figure 6. Engagement geometry for case 1.

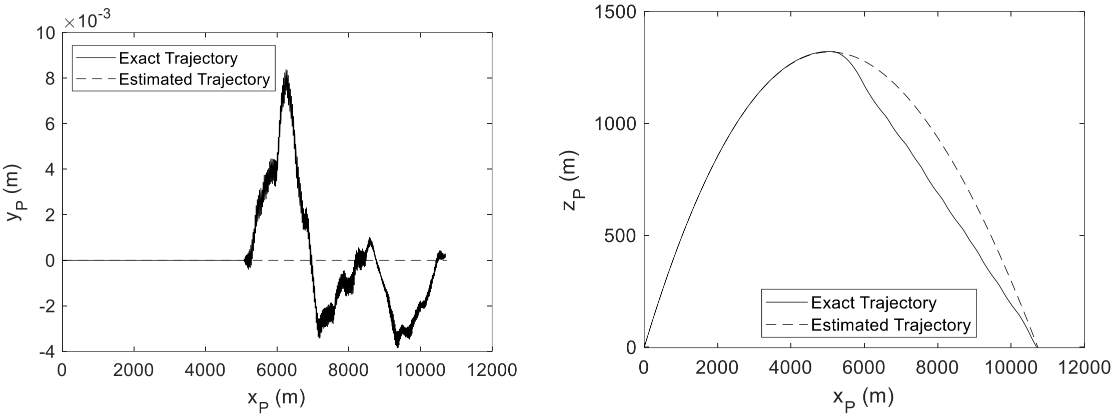

Horizontal Engagement *Vertical Engagement*

Figure 7. Engagement geometry for case 3.

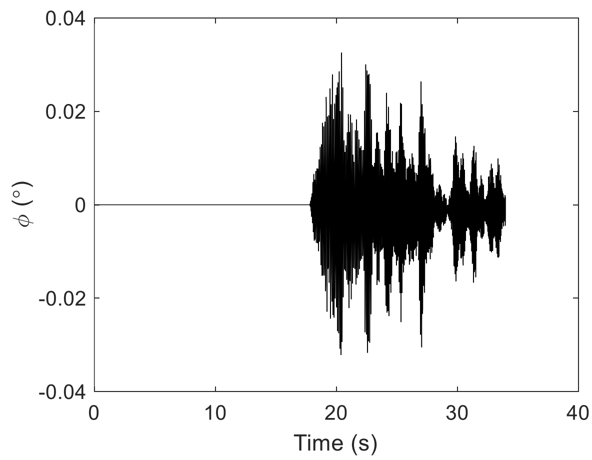

Figure 8. Change of the roll angle in time for case 3.

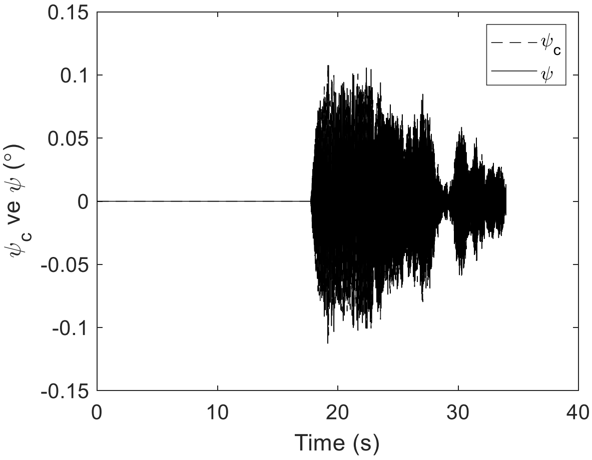

Figure 9. Time response of yaw autopilot for case 3.

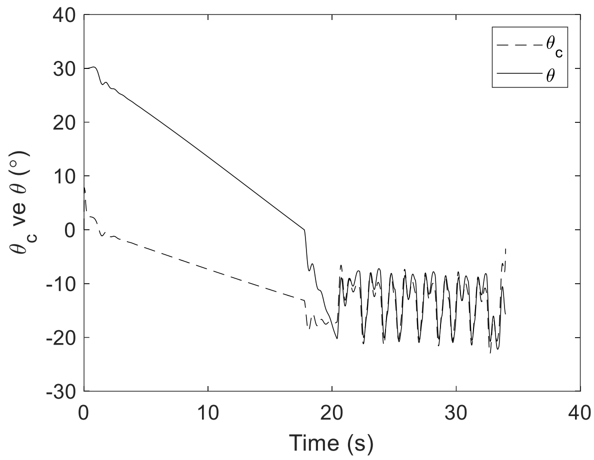

Figure 10. Time response of pitch autopilot for case 3.

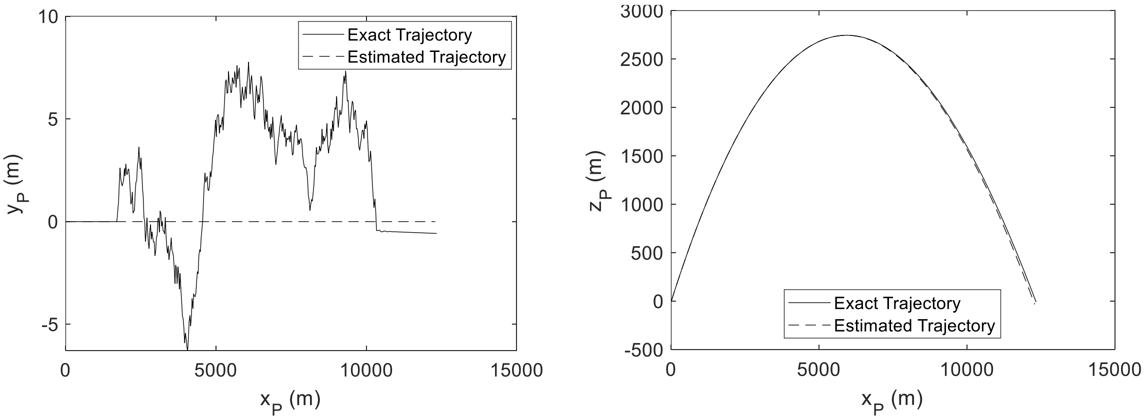

Horizontal Engagement *Vertical Engagement*

Figure 11. Engagement geometry for case 7.

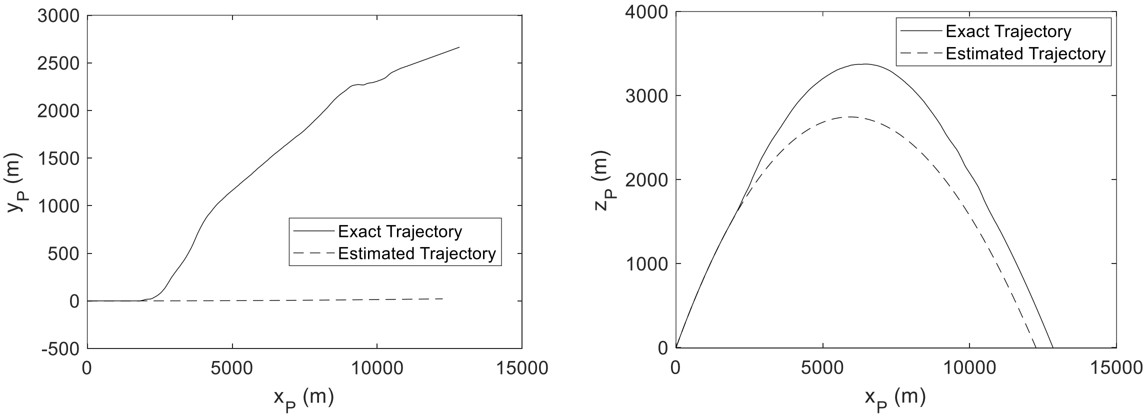

Horizontal Engagement *Vertical Engagement*

Figure 12. Engagement geometry for case 11.

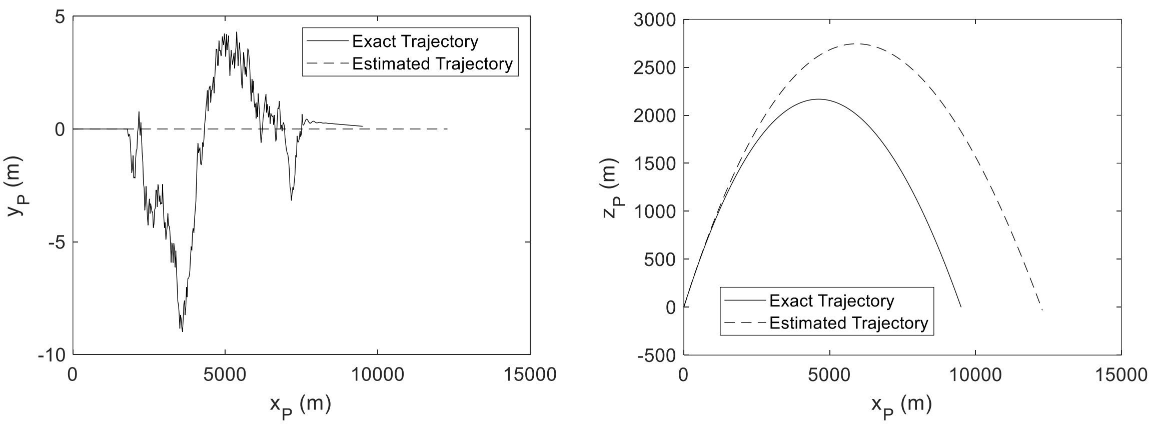

Horizontal Engagement *Vertical Engagement*

Figure 13. Engagement geometry for case 16.

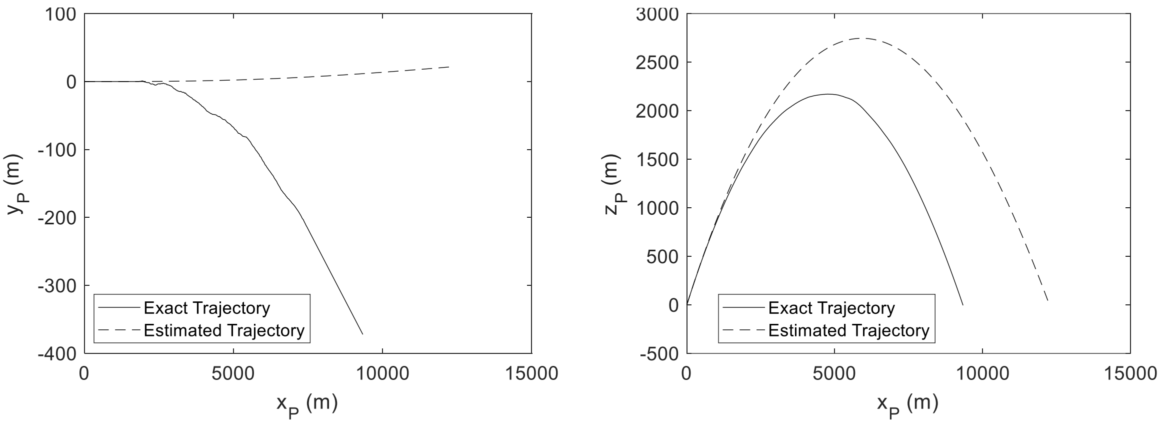

Horizontal Engagement *Vertical Engagement*

Figure 14. Engagement geometry for case 17.

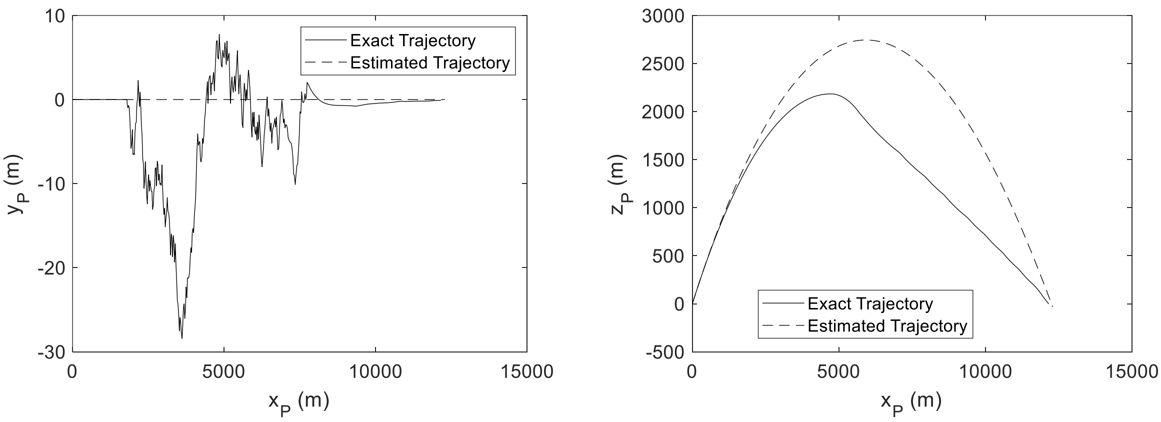

Horizontal Engagement *Vertical Engagement*

Figure 15. Engagement geometry for case 21.

6. Discussion and Conclusion

When the data acquired from the computer simulations in Table 2 and Table 3 are examined, it is observed that the guided projectile does not have any certain advantage over its unguided, or ballistic, counterparts independent of the initial pitch angle value provided that no lateral wind effect and thrust uncertainty occur. However, once the speed of the lateral wind becomes different from zero, the guided configuration leads considerably small resultant miss distances. This superiority is more apparent when the thrust of the projectile has nonzero uncertainty. That is, the supplementation of guidance makes the resultant miss distance drop down to very low values when the thrust uncertainty comes into the picture.

Here, one of the interesting points is that the guided projectile completes the engagement within almost the same duration independent of the wind existance for a specified initial pitch angle and thrust uncertainty conditions. That duration becomes longer than the engagement times yielded by the unguided projectiles in the scenarios with thrust uncertainty, but it is concluded with comparatively small miss distances from the target point.

Comparing the unguided projectiles in between, the configuration with nonzero cant angle yields smaller miss distance when there is no lateral wind effect. However, the occurrence of the wind causes the projectile with nonzero cant angle to divert more easily from its planned trajectory than the zero-cant-angle configuration. That is, it seems that the continuous high spin rate provides an unguided SSP with stability for clear weather conditions, but the spin can be a disadvantage when the projectile is subjected to side wind effect.

In the sense of the proposed gradual guidance and control strategy, the results of the computer simulations demonstrate that the roll, or spin, rate of the projectile can be zeroed within a short time interval by the constant nonzero fin deflections of NAK. In the following stage, the designed pitch and yaw autopilots track varying guidance commands accurately even under the effect of side wind.

It is evaluated that the use of a simpler, lighter, and cheaper pneumatic actuation in accordance with a convenient guidance law can make this method a viable choice for SSP applications in accordance with the yielded satisfactory miss distance and comparable engagement time results. It will be more beneficial if the simulation results can be verified by means of well-planned experimental tests as done in some of the previous studies [17].

References

[1] F. Fresconi, G. Cooper, I. Celmins, J. DeSpirito, M. Costello, "*Flight mechanics of a novel guided spin-stabilized projectile concept*" Proc. ImechE, Part G: Journal of Aerospace Engineering, 226: 327-340, 2011.

[2] F. Fresconi, I. Celmins, "*Experimental flight characterization of spin stabilized projectiles at high angle of attack*" US Army Research Laboratory Report, USA, 2017.

[3] M. D. Ilg, Guidance, "*Navigation, and control for munitions*" PhD Thesis, Drexel University, USA, 2008.

[4] J. Rogers, M. Costello, "*Design of a roll stabilized mortar projectile with reciprocating canards*" Journal of Guidance, Control, and Dynamics, 33(4): 1026-1034, 2010.

[5] Y. Qing, L. Chunsheng, "*A differential game-based guidance law for an accelerating exoatmospheric missile*" Asian Journal of Control, 19(3): 1205-1216, 2017.

[6] G. Jiwei, C. Yuan-Li Cai, "*Three-dimensional impact angle constrained guidance laws with fixed time convergence*" Asian Journal of Control, 19(6): 2240-2254, 2017.

[7] M. Eroğlu, "*Design and control of nose actuation kit for position correction of spin stabilized munitions under wind effect*" MSc Thesis, Middle East Technical University, Ankara, Turkey, 2016.

[8] Y. Habash, "*Roll controlled guided mortar (RCGM)*" NDIA Joint Armaments Conference, Seattle, WA, USA, 2012.

[9] D. N. Gkritzapis, D. P. Margaris, E. E. Panagiotopoulos, G. Kaimakamis, K. Siassiakos, "*Prediction of the impact point for spin and fin stabilized projectiles*" WSEAS Transactions on Information Science and Applications, 5(12): 1667-1676, 2008.

[10] D. N. Gkritzapis, E. E. Panagiotopoulos, D. P. Margaris, D. G. Papanikas, "*Modified linear theory for spinning or non spinning projectiles*" The Open Mechanics Journal, 1(1): 6-11, 2008.

[11] L. Baranowski, "*Equations of motion of a spin-stabilized projectile for flight stability testing*" Journal of Theoretical and Applied Mechanics, 51(1): 235-246, 2013.

[12] J. Yin, X. Wu, J. Lei, T. Lu, X. Liu, "*Canrds interference on the magnus effect of a fin stabilized spinning missile*" Advances in Mechanical Engineering, 10(7): 1-16, 2018.

[13] B. Özkan, "*Dynamic modeling of spin-stabilized projectiles*" 19th National Theory of Machine Symposium, İskenderun Technical University, İskenderun, Hatay, Turkey, 2019.

[14] G. R. Cooper, M. Costello, "*Trajectory prediction of spin-stabilized projectiles with a liquid payload*" Journal of Spacecraft and Rockets, 48(4): 664-670, 2011.

[15] K. D. Şahin, "*A pursuit evasion game between an aircraft and a missile*" MSc Thesis, Middle East Technical University, Ankara, Turkey, 2002.

[16] B. Özkan, M. K. Özgören, G. Mahmutyazıcıoğlu, "*Modeling of dynamics, guidance, and control systems of air-to-surface missiles*" The Journal of Defense Modeling and Simulation: Applications, Methodology, Technology, 9(2): 101-112, 2012.

[17] M. Milinović, D. Jerković, O. Jeremic, M. Kovac, "*Experimental and simulation testing of flight spin stability for small caliber cannon projectile*" Journal of Mechanical Engineering, 58(6): 394-402, 2012.